Available online at www.sciencedirect.com
ScienceDirect
Ceramics International 37 (2011) 2907–2912
CERAMICS INTERNATIONAL
www.elsevier.com/locate/ceramint

Short communication

Powder synthesis and aerosol deposition of the $BaCe_{0.9}Y_{0.1}O_{2.95}$ and $SrCe_{0.9}Y_{0.1}O_{2.95}$ phases for gas separation membrane application

Young-Hoon Yun [a,*], Song Min Nam [b]

[a] Department of Hydrogen & Fuel Cell Technology, Dongshin University, Jeonnam 520-714, Republic of Korea
[b] Department of Electronic Materials Engineering, Kwangwoon University, Seoul 139-701, Republic of Korea

Received 11 October 2010; received in revised form 13 January 2011; accepted 10 March 2011
Available online 14 April 2011

Abstract

Mixed-conducting oxide powders, $BaCe_{0.9}Y_{0.1}O_{2.95}$ (BCY) and $SrCe_{0.9}Y_{0.1}O_{2.95}$ (SCY), were prepared using a solid-state reaction method. X-ray diffraction patterns of the prepared powders showed the sharp peaks of the $BaCe_{0.9}Y_{0.1}O_{2.95}$ and $SrCe_{0.9}Y_{0.1}O_{2.95}$ phases. XRD patterns and FE-SEM morphologies of the oxide powders, fabricated by attrition milling and ball milling, were compared. The oxide powders that were prepared by attrition milling showed rather large particles and severe necking between particles in FE-SEM images as well as residual reactant ($BaCO_3$) and secondary phases ($SrCeO_3$ and CeO_2) in XRD patterns. The oxide powders prepared using ball milling showed particles under approximately 500 nm and typical XRD patterns of the $BaCe_{0.9}Y_{0.1}O_{2.95}$ and $SrCe_{0.9}Y_{0.1}O_{2.95}$ phases. Ceramic membranes of the $BaCe_{0.9}Y_{0.1}O_{2.95}$ and $SrCe_{0.9}Y_{0.1}O_{2.95}$ phases were fabricated by the aerosol deposition method using the oxide powders synthesized. Two fabricated ceramic membranes demonstrated somewhat dense morphologies and relatively fine grains in the FE-SEM surface images.

Keywords: Mixed-conducting oxide; A. Powders: solid state reaction; E. Membranes; E. Substrates

1. Introduction

Mixed-conducting (electronic and ionic conducting) dense ceramics are used in high-temperature electrochemical applications, including fuel cells, gas separation membranes, and electrocatalysis [1–3]. They can be used as electrodes in solid-state fuel cells and as dense ceramic membranes for gas separation. Gas separation membrane technology may provide the basis for improved methods of hydrogen recovery and, thus, reduce the cost associated with hydrogen production [4]. Gas separation technology using a mixed-conducting oxide membrane is of considerable interest for separating hydrogen from mixed synthesis gas (syngas, a mixture of CO_2 and H_2) created in an integrated gasification combined cycle (IGCC) system [5]. The process of hydrogen separation using a dense perovskite-based ceramic membrane starts with oxidation of hydrogen at the membrane surface. The protons and electrons generated are incorporated into the membrane material lattice and conducted to the reduction surface where the reverse reduction reaction occurs to produce pure hydrogen [6].

For preparing dense membranes, the perovskite compositions of multi-phase materials with high mixed proton and electron conductivity are optimized. Much research in the field of gas separation in solid oxide fuel cells has focused on the study of perovskite oxides exhibiting significant proton conductivity. One of these perovskite materials is aliovalent-doped barium cerate, $BaCe_{1-x}A_xO_{3-\delta}$ (A = common rare earth, $\delta = x/2$) [7,8]. The increase in proton conductivity with doping is mainly related to the creation of oxygen vacancies through the defect reaction. Each oxygen vacancy leads to the formation of two protons in the structure. The mechanism of proton migration in perovskite oxides has been determined as Grotthuss-type (free proton migration) [9].

Ceramic coating technology is required in many applications such as the fabrication of microelectromechanical systems (MEMS), displays and fuel cells. However, thick ceramic layers produced by conventional thin- or thick-film methods usually have cracks and may easily peel from the substrates. Several deposition methods based on the principle of particle impaction have already been investigated. The aerosol deposition method (ADM), based on the impact adhesion of fine particles for

* Corresponding author. Tel.: +82 61 330 3234; fax: +82 61 330 3234.
E-mail address: yunh2@dsu.ac.kr (Y.-H. Yun).

0272-8842/$36.00
doi:10.1016/j.ceramint.2011.03.074

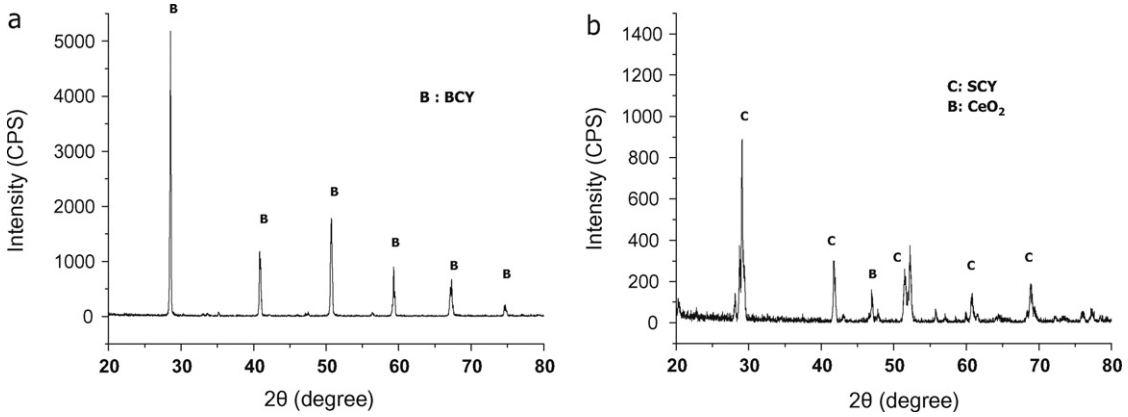

Fig. 1. XRD patterns of (a) BCY and (b) SCY powders calcined at 1100 °C for 2 h and heated at 1300 °C for 2 h after attrition milling.

forming thick ceramic layers, is utilized. In the aerosol deposition method (ADM), submicron particles are accelerated by gas flow in a nozzle and ejected onto a substrate. During impaction with the substrate, part of each particle's kinetic energy is transformed into bonding energy between particles. This process occurs without any additional source of energy. No additional procedure for the densification of the deposited layer is necessary [10–12]. Before aerosol deposition, it is very important to obtain high-purity powders with proper particle size distributions on the submicron scale (approximately ~500 nm). Generally, the cerate-based proton-conducting Ba–Ce–Y–O and Sr–Ce–Y–O materials have been synthesized by a conventional solid-state reaction method using oxide precursor powders [8,13,14].

In this study, mixed-conducting oxide powders, $BaCe_{0.9}Y_{0.1}O_{2.95}$ (BCY) and $SrCe_{0.9}Y_{0.1}O_{2.95}$ (SCY), were synthesized by a solid-state reaction method. Crystal phases of the oxide powders synthesized were identified by X-ray diffraction patterns. Microstructural morphology of the powders was observed from FE-SEM images. Dense ceramic membranes of $BaCe_{0.9}Y_{0.1}O_{2.95}$ and $SrCe_{0.9}Y_{0.1}O_{2.95}$ system were fabricated by the aerosol deposition method, respectively. Surface and cross-sectional morphologies of the ceramic membranes synthesized were observed by FE-SEM.

2. Experimental procedure

Powder samples of $BaCe_{1-x}Y_xO_{3-\delta}$ and $SrCe_{1-x}Y_xO_{3-\delta}$ ($x = 0.1$, $\delta = x/2$) were prepared by a conventional solid-state reaction from proper stoichiometric amounts of $BaCO_3$, CeO_2, $SrCO_3$ and Y_2O_3 (all Aldrich ≥99.9%). The starting oxide precursors were mixed by ball milling for approximately 24 h or attrition milling for 2 h, then passed through a 100 mesh sieve, and placed in a zirconia crucible for calcination to achieve the desired perovskite composition. Samples were calcined at 1100 °C for 2 h and then treated with a 100-mesh sieve. The final $BaCe_{0.9}Y_{0.1}O_{2.95}$ and $SrCe_{0.9}Y_{0.1}O_{2.95}$ powders were obtained by heating in a temperature range of 1100–1300 °C for 2 h in air (heating rate: 10 °C/min).

X-ray powder diffraction was performed to identify the crystal phases of the powders. Microstructural morphology of the oxide powders was observed by FE-SEM. Dense ceramic membranes of $BaCe_{0.9}Y_{0.1}O_{2.95}$ and $SrCe_{0.9}Y_{0.1}O_{2.95}$ system were fabricated by aerosol deposition method on glass substrate, respectively. Surface and cross-sectional morphologies of the ceramic membrane fabricated were observed by FE-SEM.

3. Results and discussion

3.1. XRD patterns of $BaCe_{0.9}Y_{0.1}O_{2.95}$ and $SrCe_{0.9}Y_{0.1}O_{2.95}$ powders

Fig. 1 shows XRD patterns of oxide powders fabricated by a successive process of calcination and heating after attrition

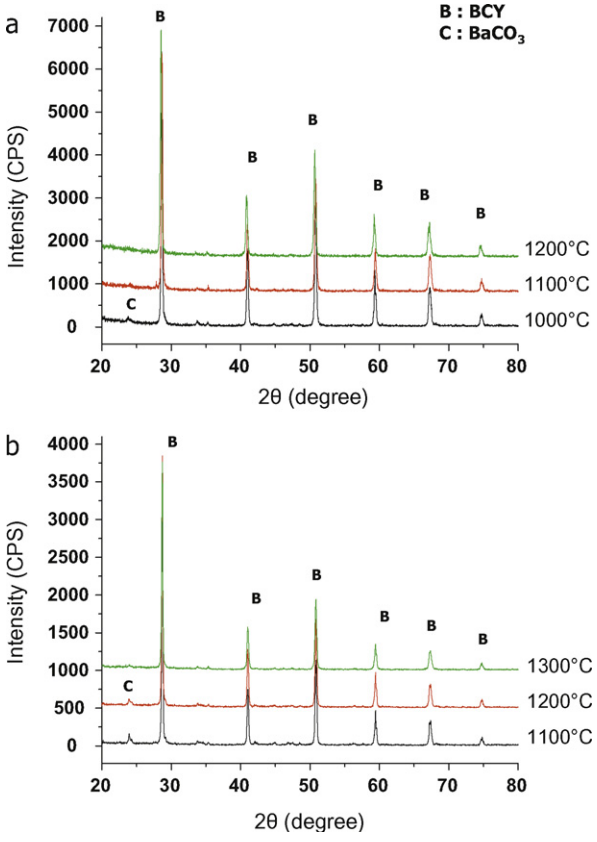

Fig. 2. XRD patterns of BCY powders prepared in temperature range of 1000–1300 °C for 2 h after (a) attrition milling and (b) ball milling.

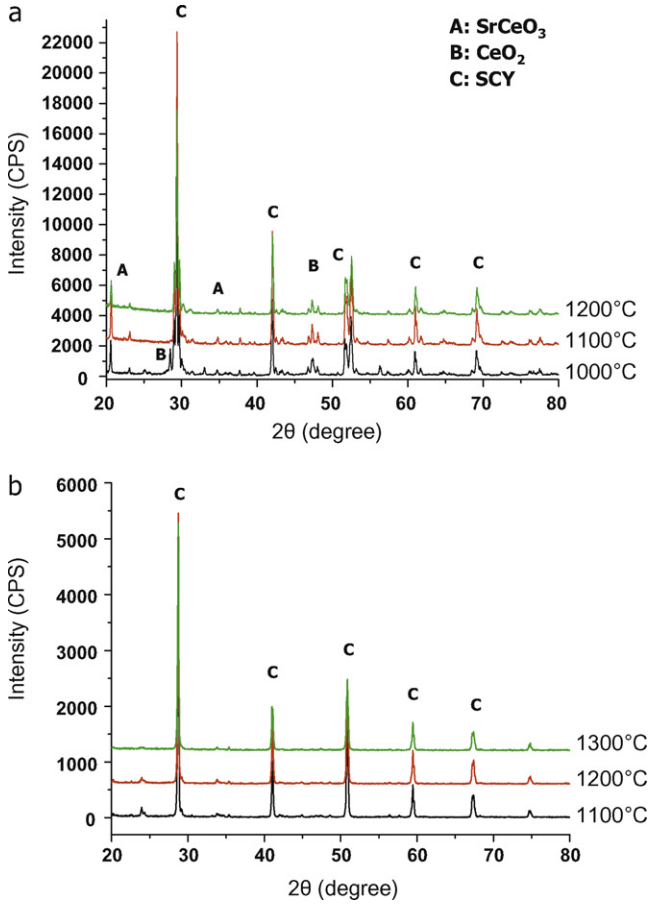

Fig. 3. XRD patterns of SCY powders prepared in temperature range of 1000–1300 °C for 2 h after (a) attrition milling and (b) ball milling.

milling. Figs. 2 and 3 show XRD patterns of the oxide powders synthesized by a single heating procedure after attrition milling and ball milling, respectively. All oxide powders synthesized by a solid-state reaction had similar XRD patterns showing the peaks of the $BaCe_{0.9}Y_{0.1}O_{2.95}$ (BCY) and $SrCe_{0.9}Y_{0.1}O_{2.95}$ (SCY) phases after heating in a temperature range of 1000–1300 °C for 2 h. The peaks of the $BaCe_{0.9}Y_{0.1}O_{2.95}$ (BCY) and $SrCe_{0.9}Y_{0.1}O_{2.95}$ (SCY) phases of two oxide powders fired showed rather strong intensity in case of the samples obtained by attrition milling compared to those obtained by ball milling. A representative orthorhombic crystal structure was confirmed for both BCY and SCY powders from all of the XRD patterns. With increasing heat treatment temperature, the XRD peak intensities of the $BaCe_{0.9}Y_{0.1}O_{2.95}$ (BCY) and $SrCe_{0.9}Y_{0.1}O_{2.95}$ (SCY) phases slightly increased. The peak of a residual BaCO3 phase after solid-state reaction was detected in the XRD patterns of the BCY oxide powder obtained at low temperature. However, in the case of attrition milling, the decomposition of the reactant phase ($BaCO_3$) during solid-state reaction was accomplished at a lower temperature (1100 °C) compared to that prepared by ball milling. Other secondary phases (Ba_2CeO_4 or CeO_2) were not detected in the XRD patterns of the powders obtained under the conditions used in the BCY powder synthesis. In XRD patterns of the SCY powders fabricated using attrition milling, even though the main peak with very strong intensity was observed, some secondary phases such as $SrCeO_3$ and CeO_2 were detected. The oxide powders, synthesized using ball milling showed typical XRD patterns of the $SrCe_{0.9}Y_{0.1}O_{2.95}$ (SCY) phase. It was inferred that mixing by attrition milling induced a somewhat incomplete formation of $SrCe_{0.9}Y_{0.1}O_{2.95}$ (SCY) during the solid-state reaction process.

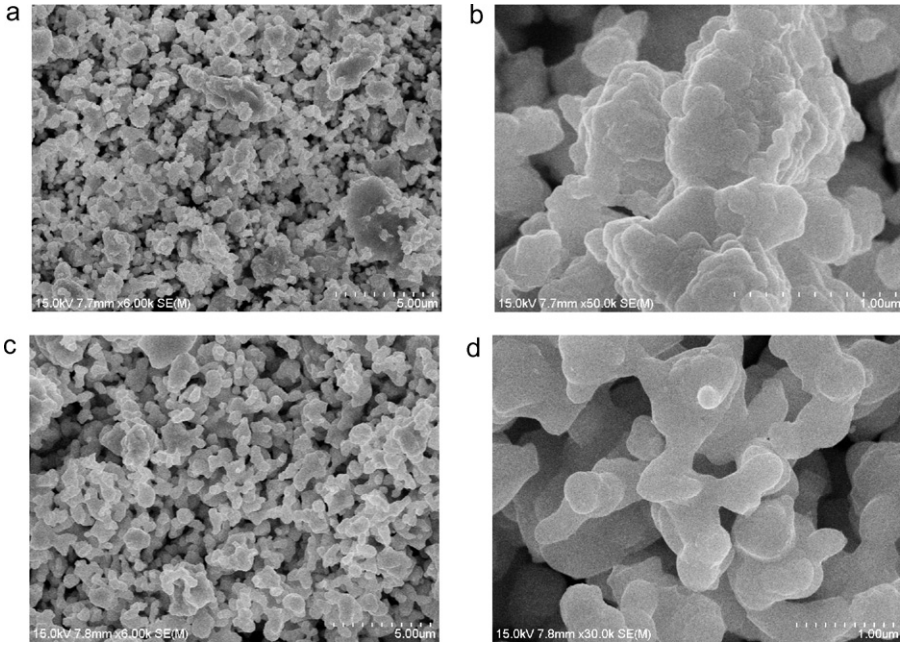

Fig. 4. FE-SEM morphologies of (a and b) BCY and (c and d) SCY oxide powders calcined at 1100 °C for 2 h and heated at 1300 °C for 2 h after attrition milling.

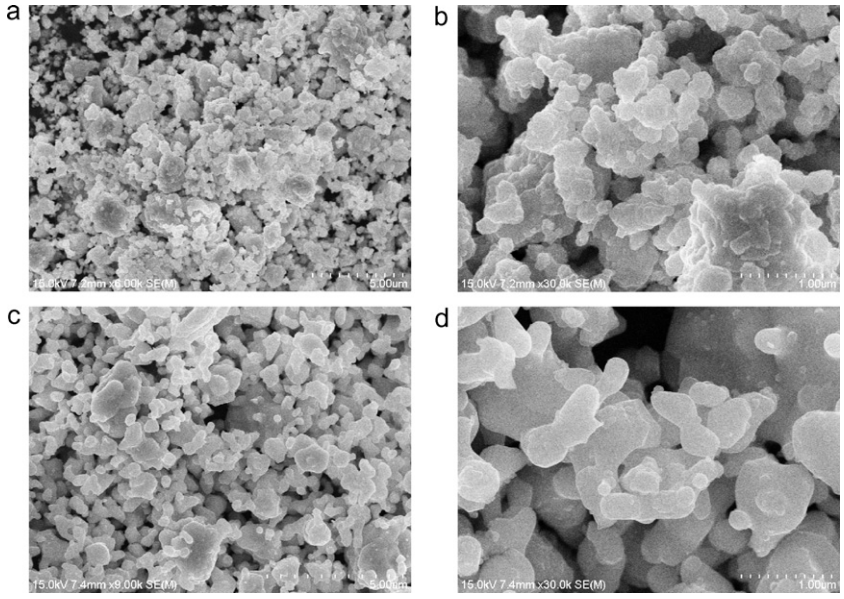

Fig. 5. FE-SEM morphologies of (a and b) BCY and (c and d) SCY oxide powders prepared at 1100 °C for 2 h after attrition milling.

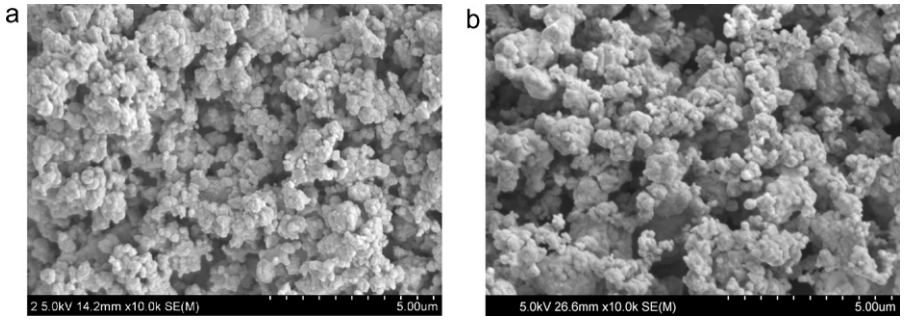

Fig. 6. FE-SEM morphologies of (a) BCY and (b) SCY oxide powders prepared at 1300 °C for 2 h after ball milling.

3.2. SEM morphologies of $BaCe_{0.9}Y_{0.1}O_{2.95}$ and $SrCe_{0.9}Y_{0.1}O_{2.95}$ powders

Fig. 4 shows the FE-SEM microstructural morphology of the oxide powders prepared by calcination and heating after attrition milling. Figs. 5 and 6 show the FE-SEM images of the $BaCe_{0.9}Y_{0.1}O_{2.95}$ (BCY) and $SrCe_{0.9}Y_{0.1}O_{2.95}$ (SCY) phases fabricated by a single heating procedure after attrition milling and after ball milling, respectively. In all oxide powders fabricated by attrition milling, relatively large particles, large aggregates, and noticeable necking between particles were observed in the FE-SEM images (Figs. 4 and 5). Powder preparation by attrition milling would have caused severe agglomeration and coarsening during solid-state reaction process. Two oxide powders, prepared by a single heating process after ball milling, showed relatively small particles, which were under approximately 500 nm. Thus, the ceramic membranes were fabricated using the oxide powders prepared by a single heating step after ball milling.

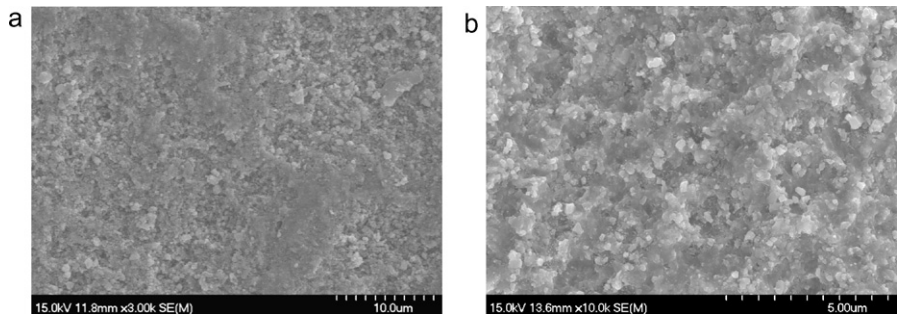

Fig. 7. FE-SEM surface morphologies of (a) BCY and (b) SCY ceramic membranes formed on glass substrate. (Oxide powders, heated at 1300 °C for 2 h after ball milling, were used for aerosol deposition.)

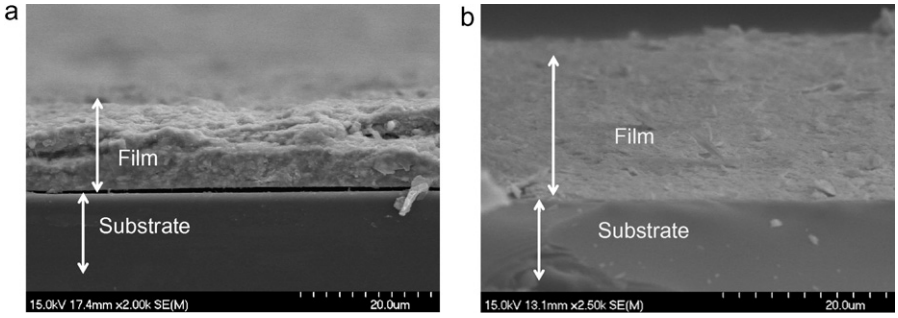

Fig. 8. FE-SEM cross-sectional morphologies of (a) BCY and (b) SCY ceramic membranes formed on glass substrate. (Oxide powders, heated at 1300 °C for 2 h after ball milling, were used for aerosol deposition.)

3.3. FE-SEM morphologies of $BaCe_{0.9}Y_{0.1}O_{2.95}$ and $SrCe_{0.9}Y_{0.1}O_{2.95}$ membranes

Fig. 7 shows surface morphologies of the ceramic membranes fabricated by an aerosol deposition process with oxide powders. The $BaCe_{0.9}Y_{0.1}O_{2.95}$ and $SrCe_{0.9}Y_{0.1}O_{2.95}$ membranes showed somewhat rough and dense morphologies in the FE-SEM surface images. However, the ceramic membranes showed relatively smaller grain sizes (of approximately 300–400 nm) compared to the particle size of the oxide powders synthesized by solid-state reaction. The densification behavior and fine grains of the ceramic membranes could be explained by the impact adhesion and bonding of the particles ejected onto the glass substrate. During a strong impact and adhesion process onto the substrate, numerous particles and large aggregates would have broken into many small pieces.

Fig. 8 shows the cross-sectional morphologies of $BaCe_{0.9}Y_{0.1}O_{2.95}$ and $SrCe_{0.9}Y_{0.1}O_{2.95}$ membranes by FE-SEM. The $BaCe_{0.9}Y_{0.1}O_{2.95}$ membrane shows rough, dense morphology and a large gap in the interface region between the membrane and substrate. The $SrCe_{0.9}Y_{0.1}O_{2.95}$ membrane shows uniform, dense morphology and excellent adhesion behavior with the substrate. The $BaCe_{0.9}Y_{0.1}O_{2.95}$ and $SrCe_{0.9}Y_{0.1}O_{2.95}$ ceramic membranes fabricated by aerosol deposition process showed different adhesion behavior to the substrate, respectively. The presence of the large gap between ceramic membrane and substrate would be due to somewhat minute shape change such as a warping or distortion of the thick ceramic membrane being applied to substrate through a high-speed impact adhesion. It appears during forming membrane that the interaction between membrane and substrate is related to several factors such as physical characteristics of the powders or substrates used.

4. Conclusion

Two oxide powders of the $BaCe_{0.9}Y_{0.1}O_{2.95}$ and $SrCe_{0.9}Y_{0.1}O_{2.95}$ phases were synthesized through a solid-state reaction from the oxide precursors $BaCO_3$, CeO_2, $SrCO_3$ and Y_2O_3. In mixing the starting materials, attrition milling was employed to form the oxide phases at a lower temperature. However, the oxide powders prepared after attrition milling showed large aggregates due to coarsening and necking of particles during heating process. The presence of secondary phases ($SrCeO_3$ and CeO_2), observed in XRD patterns indicates the incomplete solid-state reaction in the case of powder synthesis using attrition milling. The oxide powders fabricated by a single heating procedure after ball milling showed particles under approximately 500 nm and producing only the $BaCe_{0.9}Y_{0.1}O_{2.95}$ and $SrCe_{0.9}Y_{0.1}O_{2.95}$ phases in the XRD patterns. The oxide powders, prepared using ball milling were utilized to fabricate the ceramic membranes by the aerosol deposition method. The $BaCe_{0.9}Y_{0.1}O_{2.95}$ and $SrCe_{0.9}Y_{0.1}O_{2.95}$ membranes showed somewhat rough, dense morphologies and relatively small grain sizes of approximately 300 nm to 400 nm in the FE-SEM surface images. The $SrCe_{0.9}Y_{0.1}O_{2.95}$ membrane showed uniform and excellent adhesion behavior with the substrate.

Acknowledgements

This work was supported by the * *Energy Efficiency & Resources* of the Korea Institute of Energy Technology Evaluation and Planning (KETEP) grant funded by the Korea government Ministry of Knowledge Economy (No. 2008-C-CD11-P-06-1-000).

References

[1] H. Iwahara, T. Esaka, H. Uchida, N. Maeda, Proton conduction in sintered oxides and its application to steam electrolysis for hydrogen production, Solid State Ionics 3–4 (10) (1981) 359–363.
[2] U. Balachandran, B. Ma, J. Guan, P.S. Maiya, J.T. Dusek, J.J. Picciolo, S.E. Dorris, Mixed-conducting dense ceramics for gas separation applicatoins, in: Proceedings of Symposium on Solid State Ionic Devices, 195th Meeting of the Electrochemical Society, Seattle, May 2–7, 1999.
[3] M.M. Shah, R.F. Drnevich, U. Balachandran, Integrated ceramic membrane system for hydrogen production, in: Proceedings of 2000 Hydrogen Program Review, California, September 28, 2000.
[4] J. Guan, S.E. Dorris, U. Balachandran, M. Liu, The effects of dopants and A:B site nonstoichiometry on properties of perovskite-type proton conductors, J. Electrochem. Soc. 145 (5) (1998) 1780–1786.
[5] K. Xie, R. Yan, X. Liu, The chemical stability and conductivity of $BaCe_{0.9-x}Y_xSn_{0.1}O_{3-\delta}$ solid proton conductor for SOFC, J. Alloys Compd. 479 (1–2) (2009) L36–L39.
[6] G. Chiodelli, L. Malavasi, C. Tealdi, S. Barison, M. Battagliarin, L. Doubova, M. Fabrizio, C. Mortalò, R. Gerbasi, Role of synthetic route on the transport properties of $BaCe_{1-x}Y_xO_3$ proton conductor, J. Alloys Compd. 470 (1–2) (2009) 477–485.

[7] K.S. Rothenberger, A.V. Cugini, R.V. Siriwardance, D.V. Martello, J.A. Poston, E.P. Fisher, W.J. Graham, U. Balachandran, S.E. Dorris, Performance testing of hydrogen transport membranes at elevated temperatures and pressures, in: Proceedings of Symposium on Hydrogen Production, Storage, and Utilization, New Orleans, August 22–26, 1999.

[8] U. Balachandran, T.H. Lee, S.E. Dorris, Development of mixed-conducting ceramics membrane for hydrogen separation, in: 100th Annual Meeting and Exposition of the American Ceramic Society, Cincinnati, May 3–6, 1998.

[9] S.E. Roark, T.F. Sammells, A. Calihman, A. Girard, P.M.V. Calcar, R. Mackay, T. Barton, S. Rolfe, Advanced hydrogen transport membranes for VISION 21 FOSSIL FUEL PLANTS, Technical Report of Eltron Research Inc., Colorado, January 30, 2001.

[10] J. Akedo, M. Lebedev, A. Iwata, H. Ogiso, S. Nakano, Aerosol deposition method (ADM) for nano-crystal ceramics coating without firing, Mater. Res. Soc. Symp. Proc. 779 (2003) 289–299.

[11] J. Akedo, Aerosol deposition method for fabrication of nano crystal ceramic layer, Mater. Sci. Forum 449–452 (2004) 43–48.

[12] J. Akedo, Aerosol deposition of ceramic thick films at room temperature: densification mechanism of ceramic layers, J. Am. Ceram. Soc. 89 (6) (2006) 1834–1839.

[13] M. Oishi, S. Akoshima, K. Yashiro, K. Sato, J. Mizusaki, T. Kawada, Defect structure analysis of B-site doped perovskite-type proton conducting oxide $BaCeO_3$. Part 1. The defect concentration of $BaCe_{0.9}M_{0.1}O_{3-\delta}$ (M = Y and Yb), Solid State Ionics 180 (2–3) (2009) 127–131.

[14] J. Lv, L. Wang, D. Lei, H. Guo, R.V. Kumar, Sintering, chemical stability and electric conductors $BaCe_{0.45}Zr_{0.45}M_{0.1}O_{3-\delta}$ (M = In, Y, Gd, Sm), J. Alloys Compd. 467 (1–2) (2009) 376–382.